Two-dimensional Hubbard model: Numerical simulation study

J. E. Hirsch
Department of Physics, University of California, San Diego, La Jolla, California 92093
(Received 1 October 1984)

We have studied the two-dimensional Hubbard model on a square lattice with nearest-neighbor hopping. We first discuss the properties of the model within the mean-field approximation: Because of the form of the band structure, some peculiar features are found. We then discuss the simulation algorithm used and compare simulation results with exact results for 6-site chains to test the reliability of the approach. We present results for thermodynamic properties and correlation functions for lattices up to 8×8 in spatial size. The system is found to be an antiferromagnetic insulator for all values of the coupling constant at zero temperature in the half-filled-band case, but the long-range order is much smaller than predicted by mean-field theory. We perform a finite-size-scaling analysis to determine the character of the transition at zero coupling. For non-half-filled-band cases, our results suggest that the system is always paramagnetic, in contradiction with Hartree-Fock predictions. The system does not show tendency to ferromagnetism nor triplet superconductivity in the parameter range studied. We also discuss some properties of the attractive Hubbard model in the half-filled-band case.

I. INTRODUCTION

The Hubbard model[1] is defined by the lattice Hamiltonian:

$$H=\sum_{\substack{i,j\\ \sigma}} t_{ij}(c_{i\sigma}^{\dagger}c_{j\sigma}+\text{H.c.})+U\sum_i n_{i\uparrow}n_{i\downarrow}-\mu\sum_i (n_{i\uparrow}+n_{i\downarrow})\ . \tag{1.1}$$

It describes a single s band in a tight-binding basis, with a local electron-electron repulsion U for electrons of opposite spin at the same atomic orbital. The model is thought to be appropriate to describe the main features of electron correlations in narrow energy bands, leading to collective effects such as itinerant magnetism and metal-insulator transition, and has been often used to describe real materials exhibiting these phenomena.[2] A detailed justification for Eq. (1) as a model for narrow-band systems has been given by Hubbard.

Although simple in appearance, the model cannot be solved exactly except in one dimension.[3] Even there, the exact solution provides only partial information about the system. In more than one dimension, the model is not exactly solvable and a variety of approximate techniques have been used to study it, among others mean-field theory,[4] Green's-function decoupling schemes,[1] functional integral formulations,[5] and variational approaches.[6] These techniques are uncontrolled (except perhaps for weak coupling) and often give conflicting results, so that it is fair to say that no general agreement exists on what the properties of the model are.

An important approach to the problem is the study of (small) finite systems. In one dimension, this was first done by Shiba and Pincus for chains of up to 6 sites.[7] More recently, exact diagonalization of chains of up to 12 sites have been performed.[8] Because in exact diagonalizations the computer time needed for a calculation increases exponentially with the size of the system, the method becomes of limited use in more than one dimension. Results for higher-dimensional lattices have been recently reported by Kawabata[9] (for systems of up to 8 sites) and by Takahashi[10] for the somewhat simpler case where $U=\infty$ (up to 12-site systems). However, these systems are too small to allow one to draw conclusions about the properties of the model in the thermodynamic limit.

An alternative method to study finite lattices is Monte Carlo simulations. In one dimension, an algorithm exists where the computer time increases *linearly* with the size of the system,[11] and chains of up to 40 sites have been studied with modest amounts of computer time.[11–13] In more than one dimension, no algorithm where the computer time increases linearly with the size is known. Here, we have used a discrete Hubbard-Stratonovich transformation to convert the problem into one of free electrons interacting with a time-dependent Ising field,[14] together with an exact updating algorithm for the fermion Green's function[15] to compute the relative weights of the Ising configurations. The computer time in this algorithm increases with the *cube* of the size of the system, and we have used it to study lattices of up to 64 sites (8×8 two-dimensional lattices). This is well beyond the reach of exact diagonalization techniques at present, and large enough to allow us to draw some conclusions about the infinite system. We have recently reported results of simulations on this model in a short communication.[16] Here, we discuss the approach in more detail and present additional results.

We discuss results of our study for the two-dimensional square lattice with nearest-neighbor hopping only. The properties of the model are sensitive to the band structure, and two distinct features of our model in the half-filled-band case, namely nesting of the Fermi surface and a singularity in the density of states at the Fermi energy, determine much of its properties. A different band struc-

ture (including next-nearest-neighbor hopping, for example) should have rather different properties, and will be discussed in a future publication. This feature of fermion models restricts the "universality classes" more than, for example, in classical spin models, where the properties are usually independent of the details of the short-range couplings. Nevertheless, we believe our results for the half-filled band should apply at least qualitatively for models with nested Fermi surface. For the non-half-filled band, we believe our conclusions are quite general.

We compare our results with predictions of Hartree-Fock theory, thus illustrating the effect of fluctuations in changing the mean-field solution. A comparison with more sophisticated approximate theories provides information about the reliability of these schemes and will be discussed elsewhere.

The main question addressed in this paper concerns magnetism due to itinerant electrons. Can the Hubbard model provide a sensible description of it? Because our model is two dimensional, we can only have magnetic long-range order in the ground state; at $T>0$, a continuous symmetry cannot be broken in two dimensions. We find that the model does exhibit long-range antiferromagnetic order in the ground state for the half-filled-band case, even in the presence of a substantial delocalization of the electrons. The system, however, does not show "metallic magnetism:" only for the insulating half-filled case there appears to be magnetic long-range order. In addition, it does not display any tendency to *ferromagnetic* correlations, let alone ferromagnetism, in the range of interaction and band filling studied. We believe that with a modified band-structure tendency to ferromagnetism could be enhanced, but it is unlikely that ferromagnetic long-range order will appear. We also do not find any tendency towards triplet or singlet pairing in our model.

Concerning the metal-insulator transition, the model discussed here is an insulator for any $U>0$ (in the half-filled case) due to the nesting of the Fermi surface. In that respect, the model is similar to the one-dimensional Hubbard model where nesting always occurs.

The paper is organized as follows. In the next section we discuss some features of the model in the noninteracting case, the Hartree-Fock solution, and the strong-coupling limit. In Sec. III we discuss the simulation method used and compare simulation results with exact results for a 6-site system with the exact diagonalization results of Shiba, to test the reliability of our approach. In Sec. IV we present results of simulations for the half-filled case, and in Sec. V for some non-half-filled band cases. We discuss briefly the implications of our results for the two-dimensional attractive Hubbard model in Sec. VI, and summarize our conclusions in Sec. VII.

II. THE MODEL

We consider the model defined by the Hamiltonian:

$$H=-t\sum_{\substack{\langle i,j\rangle\\ \sigma}}(c_{i\sigma}^{\dagger}c_{j\sigma}+\text{H.c.})+U\sum_i n_{i\uparrow}n_{i\downarrow}-\mu\sum_i(n_{i\uparrow}+n_{i\downarrow}) , \tag{2.1}$$

where $\langle i,j\rangle$ denotes nearest neighbors and the sum runs over sites of a two-dimensional square lattice. The chemical potential μ is $U/2$ for a half-filled band. We consider here the case of repulsive interactions ($U\geq 0$).

The single-particle eigenstates for the noninteracting case ($U=0$) have energies

$$\epsilon_k=-2t(\cos k_x+\cos k_y)-\mu ,$$
$$k_{x,y}=\frac{2\pi}{N_{x,y}}n_{x,y},\quad \frac{-N_{x,y}}{2}\leq n_{x,y}<\frac{N_{x,y}}{2} , \tag{2.2}$$

so that the bandwidth is $W=8t$. The ground state for the noninteracting system is obtained by filling the negative energy states. Figure 1 shows the Fermi surface for various band fillings for an infinite two-dimensional lattice. The Fermi surface in the half-filled case is "nested," i.e., a reciprocal-lattice vector $[(\pi/a,\pi/a)$ or $(-\pi/a,\pi/a)]$ maps an entire section of the Fermi surface onto another. This is due to the fact that our lattice is bipartite, and the kinetic energy connects only one sublattice to the other. As is well known, this has important consequences for the properties of the model.[17]

Another important feature of the noninteracting system appears in the density of states, defined by

$$g(\epsilon)=\sum_k\delta[\epsilon-\epsilon(k)] , \tag{2.3}$$

which is shown in Fig. 2. The density of states displays a logarithmic singularity $g(\epsilon)\sim\ln(\epsilon/4t)$ for small ϵ. From topological arguments, one can show that such a singularity will always occur in a two-dimensional system. However, the fact that it occurs at the Fermi energy for the half-filled case, for the same energy where nesting occurs, is special to the nearest-neighbor-hopping model considered here.

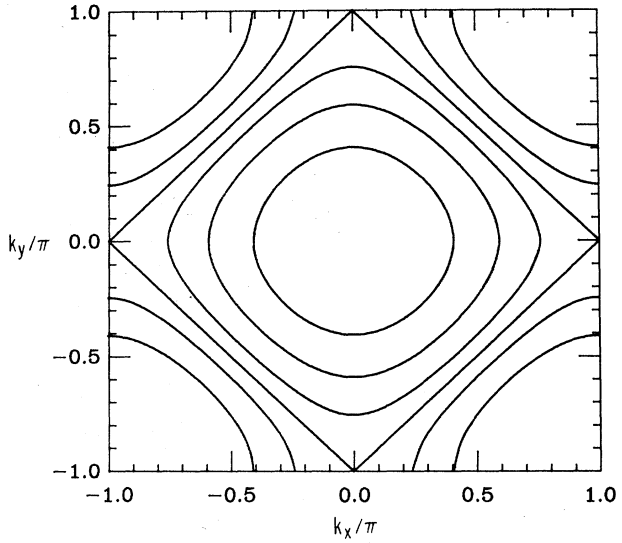

FIG. 1. Fermi surfaces for electrons on a two-dimensional square lattice with nearest-neighbor hopping only. Band fillings are $\rho=0.25, 0.5, \ldots, 1.5$ starting from the inner surface. Note that the Fermi surface for the half-filled case is nested.

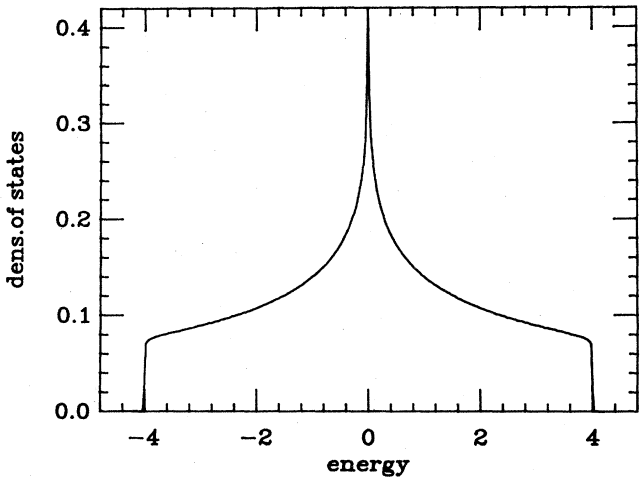

FIG. 2. Density of states for noninteracting electrons on a two-dimensional square lattice with nearest-neighbor hopping. The singularity at the origin is logarithmic.

The q-dependent zero-frequency susceptibility (per spin) for the noninteracting case is given by

$$\chi_0(q)=-\frac{1}{N}\sum_k \frac{f(\epsilon_{k+q})-f(\epsilon_k)}{\epsilon_{k+q}-\epsilon_k} \tag{2.4}$$

with $f(\epsilon)$ the Fermi function:

$$f(\epsilon)=\frac{1}{e^{\beta\epsilon}+1} . \tag{2.5}$$

For $q=0$, we have

$$\chi_0(q=0)=\int d\epsilon g(\epsilon)\frac{\partial f}{\partial \epsilon}\underset{T\to 0}{\to} g(\epsilon_F) , \tag{2.6}$$

i.e., the usual Pauli result. In the half-filled case, the susceptibility diverges as $T\to 0$ due to the singularity in the density of states, as

$$\chi_0(q=0)\sim -\ln\left[\frac{T}{t}\right] . \tag{2.7}$$

The staggered susceptibility is given by

$$\chi_0(q=\pi)=\frac{1}{N}\sum_k \frac{f(-\epsilon_k)-f(\epsilon_k)}{2\epsilon_k} = \int d\epsilon g(\epsilon)\frac{f(-\epsilon)-f(\epsilon)}{2\epsilon} . \tag{2.8}$$

In the usual case where one has a nested Fermi surface this gives a logarithmic divergence of the susceptibility at low temperatures. Here, however, we have in addition the singularity in the density of states, and the low-temperature behavior in the half-filled case is

$$\chi_0(q=\pi)\sim \left[\ln\frac{T}{t}\right]^2 , \tag{2.9}$$

i.e., a stronger divergence than for the $q=0$ susceptibility. For the non-half-filled case, the q-dependent susceptibility is finite as $T\to 0$.

For nonzero U, the magnetic susceptibility within the random-phase approximation (RPA) is given by the sum of particle-hole ladder diagrams[18] as

$$\chi(q)=\frac{2\chi_0(q)}{1-U\chi_0(q)} . \tag{2.10}$$

For the half-filled case, the divergences in χ_0 indicate instabilities for arbitrarily small values of U at both $q=0$ and $q=(\pi,\pi)$. Because the divergence in χ_0 is stronger for $q=(\pi,\pi)$, RPA predicts a transition to an antiferromagnetic phase at a higher temperature than for the ferromagnetic phase in the half-filled case. For the non-half-filled case, RPA predicts a transition at a *finite* value of U, since the susceptibility is nondivergent. The transition will be to states defined by the wave vector q for which χ_0 is maximum, which is a decreasing function of the band filling. However, because we are dealing with a two-dimensional model with a continuous symmetry, it is clear that no transition to a state with magnetic long-range order can occur expect possibly for $T=0$.

We now discuss the Hartree-Fock (HF) solution for this model. This has been discussed in detail by Penn for the three-dimensional case.[4] Within the Hartree-Fock approximation, the Hamiltonian is

$$H_{\rm HF}=-t\sum_{\langle i,j\rangle,\sigma} c_{i\sigma}^{\dagger}c_{j\sigma} +U\sum_i (\langle n_{i\uparrow}\rangle n_{i\downarrow}+n_{i\uparrow}\langle n_{i\downarrow}\rangle-\langle n_{i\uparrow}\rangle\langle n_{i\downarrow}\rangle) -\mu\sum_i (n_{i\uparrow}+n_{i\downarrow}) . \tag{2.11}$$

For the half-filled case, the appropriate solution is the antiferromagnetic one:

$$\langle n_{i\uparrow}\rangle=n+(-1)^i m , \qquad \langle n_{i\downarrow}\rangle=n-(-1)^i m , \tag{2.12}$$

which yields the gap equation:

$$1=\frac{U}{4\pi^2}\int d^2k\frac{1}{(\epsilon_k^2+\Delta^2)^{1/2}} , \tag{2.13a}$$

$$\Delta=Um , \tag{2.13b}$$

which has a solution with $m\neq 0$ for arbitrarily small U due to the nesting of the Fermi surface. The features of the singularity are, however, different from the usual case. Rewriting Eq. (2.13a) as

$$1=U\int_0^{4t} d\epsilon\frac{\rho(\epsilon)}{(\epsilon^2+\Delta^2)^{1/2}} \tag{2.14}$$

and due to the singularity in the density of states, we find for the gap

$$\Delta\sim te^{-2\pi\sqrt{t/U}} \quad (d=2) . \tag{2.15}$$

In contrast, both in one and three dimensions there is no singularity at the Fermi energy for the half-filled case, and the gap within HF behaves as

$$\Delta \sim te^{-2\pi t/U} \quad (d=1,3) . \tag{2.16}$$

This particular feature of the model under consideration gives a stronger tendency to antiferromagnetic ordering than in the usual case.[19] It should be remarked that the behavior, Eq. (2.15), is a consequence of the fact that both the nesting of the Fermi surface and the Van Hove singularity in the density of states occur at the same energy, the Fermi energy for the half-filled case. One can easily construct other band structures in $d=2$ where both features occur at different energies, or where the nesting is absent altogether, which will then have rather different properties. The logarithmic singularity, however, is required by topology in $d=2$ so that it always occurs. In the absence of nesting, it may give a tendency for ferromagnetic correlations.

For the non-half-filled band case we consider, in addition to (2.12), the possibility of ferromagnetic solutions:

$$\begin{aligned} \langle n_{i\uparrow}\rangle &= n+m , \\ \langle n_{i\downarrow}\rangle &= n-m , \end{aligned} \tag{2.17}$$

and paramagnetic ones, with $m=0$. The Hartree-Fock phase diagram, obtained by choosing the solution that gives the lowest energy (if more than one solution exists) is shown in Fig. 3, and is rather similar to the one obtained in $d=3$ by Penn. Note that for large U and fillings close to 1 ferromagnetism is predicted to occur. This is also in agreement with the exact results by Nagaoka,[20] who found the ferromagnetic state to be the ground state for $U=\infty$ and one hole in a half-filled-band system. However, we will see that our simulations do not give any indication that there is a tendency towards ferromagnetic ordering.

Finally, we review the strong-coupling limit of the model Eq. (2.1) for the half-filled-band case. To second order in the hopping the model is equivalent to an antiferromagnetic Heisenberg model, defined by the Hamiltonian

$$H_{\text{eff}} = +\frac{4t^2}{U} \sum_{\langle i,j\rangle} \mathbf{S}_i \cdot \mathbf{S}_j \tag{2.18}$$

with $\mathbf{S}$ the Pauli matrices. According to the finite lattice calculations of Oitmaa and Betts,[21] this model has antiferromagnetic long-range order in the ground state, approximately 50% reduced from the classical Néeel state due to quantum fluctuations. The existence of long-range antiferromagnetic order for the case $0<U<\infty$, where both spin and charge fluctuations occur, was an open question; in this work we believe we have established that the model indeed has antiferromagnetic order for $0<U<\infty$ in the half-filled-band case.

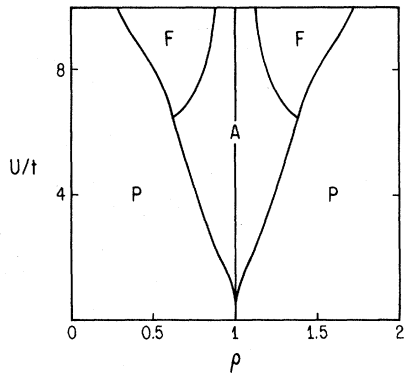

FIG. 3. Hartree-Fock phase diagram for the two-dimensional Hubbard model. A, F, and P denote antiferromagnetic, ferromagnetic, and paramagnetic ground states, respectively.

The behavior of the magnetic susceptibility at low temperatures in the limit where Eq. (2.18) is valid follows from a spin-wave analysis. Assuming a linear dispersion relation for the spin-wave energy, $\epsilon(k)\sim ck$, we obtain

$$\chi \sim \frac{1}{T} \int kdk \frac{e^{\beta k}}{(e^{\beta k}-1)^2} \sim T \ln T \tag{2.19}$$

at low temperatures. The staggered susceptibility should be the same as the susceptibility for a ferromagnet, with $\epsilon(k)\sim ck^2$, and yields

$$\chi(q=2k_F) \sim \frac{1}{T} , \tag{2.20}$$

which happens to be the same as the Curie law because we are in two dimensions. Note that the susceptibility in the large-U limit vanishes as $T\to 0$ [Eq. (2.19)], in contrast to the $U=0$ limit where it diverges [Eq. (2.7)].

III. THE SIMULATION

The simulation was constructed using an Ising functional integral formulation recently introduced. The partition function is written as

$$Z = \mathrm{Tr} e^{-\beta H} = \mathrm{Tr} \prod_{l=1}^{L} e^{-\Delta\tau H} \cong \mathrm{Tr} \prod_{l=1}^{L} e^{-\Delta\tau H_0} \exp\left[-\Delta\tau \left[U \sum n_{i\uparrow} n_{i\downarrow} - \mu \sum (n_{i\uparrow}+n_{i\downarrow})\right]\right] \tag{3.1}$$

with H_0 the kinetic energy and $\beta = L\Delta\tau$. The error in the breakup in Eq. (3.1) is of order $O(\Delta\tau^2 tU)$. The electron-electron interaction was eliminated using the identity[14]

$$e^{-\Delta\tau U n_{i\uparrow} n_{i\downarrow}} = \mathrm{Tr}_\sigma \exp\left[\lambda\sigma(n_{i\uparrow}-n_{i\downarrow}) - \frac{\Delta\tau U}{2}(n_{i\uparrow}+n_{i\downarrow})\right] \tag{3.2}$$

with

$$\lambda = 2 \arctan\sqrt{\tanh(\Delta\tau U/4)} \tag{3.3}$$

and $\sigma=\pm 1$. The partition function is then

$$Z=\mathrm{Tr}_\sigma \mathrm{Tr}\prod_{l=1}^{L} e^{-\Delta\tau H_0}\exp\left[\lambda\sigma(n_{i\uparrow}-n_{i\downarrow})-\Delta\tau(\mu-U/2)(n_{i\uparrow}+n_{i\downarrow})\right]$$
$$=\mathrm{Tr}_\sigma \mathrm{Tr}\left[\prod_{l=1}^{L} e^{-\Delta\tau H_{0\uparrow}}\exp\{[\lambda\sigma-\Delta\tau(\mu-U/2)]n_{i\uparrow}\}\right]\left[\prod_{l=1}^{L} e^{-\Delta\tau H_{0\downarrow}}\exp\{[-\lambda\sigma-\Delta\tau(\mu-U/2)]n_{i\downarrow}\}\right] . \quad (3.4)$$

Denote

$$B_l(\alpha)=e^{-\Delta\tau K}e^{V^\alpha(l)} , \quad (3.5)$$

$$(K)_{ij}=\begin{cases}-t & \text{for } i,j \text{ nearest neighbors,}\\ 0 & \text{otherwise ,}\end{cases} \quad (3.6a)$$

$$V_{ij}^\alpha(l)=\delta_{ij}[\lambda\alpha\sigma_i(l)-\Delta\tau(\mu-U/2)] , \quad (3.6b)$$

and define the operators

$$D_l(\alpha)=e^{-\Delta\tau c_i^\dagger K_{ij}c_j}e^{c_i^\dagger V_i^\alpha(l)c_i} , \quad (3.7)$$

so that the partition function is

$$Z=\mathrm{Tr}_\sigma \mathrm{Tr}\prod_{\alpha=\pm 1}\prod_{l=1}^{L} D_l(\alpha) . \quad (3.8)$$

We can take the trace over fermions explicitly, since there are only bilinear forms in fermion operators, and obtain

$$Z=\mathrm{Tr}_\sigma\prod_\alpha \det[1+B_L(\alpha)B_{L-1}(\alpha)\cdots B_1(\alpha)]$$
$$\equiv \mathrm{Tr}_\sigma \det O_\uparrow \det O_\downarrow . \quad (3.9)$$

This identity was proved by Blankenbecler *et al.*,[15] using Grassmann variables. For the reader unfamiliar with Grassmann algebras, we give an elementary derivation of this result in the Appendix.

The remaining sum over Ising spins in Eq. (3.9) is performed using a Monte Carlo technique, taking as Boltzmann weight the product of determinants in Eq. (3.9). For the case of a half-filled band, it is easy to show that this product is positive for arbitrary σ configurations. Consider the particle-hole transformation

$$d_{i\sigma}=(-1)^i c_{i\sigma}^\dagger ,$$
$$c_{i\sigma}^\dagger c_{i\sigma}=1-d_{i\sigma}^\dagger d_{i\sigma} . \quad (3.10)$$

For the half-filled band, $\mu=U/2$ and we have from Eq. (3.4)

$$\det O_\uparrow=\mathrm{Tr}_c\prod_{i=1}^{L} e^{-\Delta\tau H_{0\uparrow}}e^{\lambda\sigma c_{i\uparrow}^\dagger c_{i\downarrow}}$$
$$=\mathrm{Tr}_d\prod_{i=1}^{L} e^{-\Delta\tau H_{0\uparrow}}e^{-\lambda\sigma d_{i\uparrow}^\dagger d_{i\downarrow}}e^{\lambda\sigma_i(l)} , \quad (3.11)$$

so that

$$\det O_\uparrow=e^{\lambda\sum_{i,l}\sigma_k(l)}\det O_\downarrow \quad (3.12)$$

and the product of determinants in Eq. (3.9) is positive definite, so that it can be used as a Boltzmann weight. For the non-half-filled band, we define the Boltzmann weight as

$$P(\sigma)=|\det O_\uparrow \det O_\downarrow| \quad (3.13)$$

and have to compute the average sign of the product of determinants. We find that the product of determinants does become negative for certain field configurations, but the average sign is always well behaved and does not go to zero rapidly as β or the lattice size increases, so that it does not represent a problem for doing Monte Carlo simulations.

We use the heat-bath algorithm to perform the sum over Ising spins. If R_α is the ratio of the new to the old determinant for fermion spin α on flipping a given Ising spin, it is flipped with probability

$$P=\frac{R_\uparrow R_\downarrow}{1+R_\uparrow R_\downarrow} . \quad (3.14)$$

To compute R_α, we use the procedure introduced by Blankenbecler, Scalapino, and Sugar[15] which involves updating the full Green's function exactly when a move is accepted. This takes the bulk of the computer time in the calculation, N^2 operations per update, with N the number of spatial sites. After several updatings, the Green's function degrades due to rounding errors and has to be recomputed from scratch. This makes a non-negligible difference in terms of computer time only if it has to be done every time slice or two. In practice, we started our simulations by recomputing G from scratch every 10 time slices and checking whether it had degraded by more than 1%. If so, we recomputed it more often, which we had to do for large values of the interaction.

We now consider the evaluation of average quantities. First, it is easy to show that[14]

$$\langle(n_{i\uparrow}(\tau)-n_{i\downarrow}(\tau))(n_{j\uparrow}(0)-n_{j\downarrow}(0))\rangle$$
$$=(1-e^{-\Delta\tau U})^{-1}\langle\sigma_i(\tau)\sigma_j(0)\rangle , \quad (3.15)$$

so that we obtain fermion spin-spin correlation functions simply from correlation functions of the Ising spins. For other correlation functions, we do not have enough information in the Ising variables but have to average over appropriate fermion matrices. For an equal time correlation of the operators P_i and Q_j we have

$$\langle\langle P_iQ_j\rangle\rangle=\frac{\mathrm{Tr}_\sigma \mathrm{Tr}P_iQ_j\prod_\alpha\prod_l D_l(\alpha)}{Z}$$
$$=\frac{\mathrm{Tr}_\sigma\langle P_iQ_j\rangle\det O_\uparrow\det O_\downarrow}{Z} , \quad (3.16)$$

$$\langle P_iQ_j\rangle=\frac{\mathrm{Tr}P_iQ_j\prod_{l,\alpha}D_l(\alpha)}{\det O^\uparrow\det O_\downarrow} . \quad (3.17)$$

It is easy to obtain the appropriate formulas by using the

transformation to normal modes, Eq. (A6), of the entire product of factors in (3.17). For example, consider the single-particle Green's functions (we omit spin indices for simplicity):

$$\langle c_i c_j^\dagger \rangle = \frac{\mathrm{Tr} c_i c_j^\dagger \prod_\nu e^{-c_\nu^\dagger l_\nu c_\nu}}{\prod_\nu (1+e^{-l_\nu})}$$

$$= \sum_{\nu'} \langle \nu' \mid i \rangle \langle j \mid \nu' \rangle \frac{\mathrm{Tr} c_{\nu'} c_{\nu'}^\dagger \prod_\nu e^{-c_\nu^\dagger l_\nu c_\nu}}{\prod_\nu (1+e^{-l_\nu})}$$

$$= \sum_{\nu'} \langle \nu' \mid i \rangle \langle j \mid \nu' \rangle \frac{1}{1+e^{-l_{\nu'}}}$$

$$= \left[\frac{1}{1+B_L B_{L-1} \cdots B_1} \right] ij \ . \tag{3.18}$$

Similarly,

$$\langle c_i^\dagger c_j \rangle = \left[B_L \cdots B_1 \frac{1}{1+B_L \cdots B_1} \right] ji \ . \tag{3.19}$$

For two-particle Green's functions, it is straightforward to show, by expanding in eigenstates, that Wick's theorem applies, i.e.,

$$\langle c_{i_1}^\dagger c_{i_2} c_{i_3}^\dagger c_{i_4} \rangle = \langle c_{i_1}^\dagger c_{i_2} \rangle \langle c_{i_3}^\dagger c_{i_4} \rangle + \langle c_{i_1}^\dagger c_{i_4} \rangle \langle c_{i_2}^\dagger c_{i_3} \rangle \ . \tag{3.20}$$

Note that this decoupling applies only to the "single-bracket" average (trace over fermions) and not to the full average, denoted by double angular brackets [Eq. (3.16)], which involves the additional trace over spins. For averages involving fermion operators of both spins we can simply factorize, since everything is diagonal in spins, for example,

$$\langle n_{i\uparrow} n_{j\downarrow} \rangle = \langle n_{i\uparrow} \rangle \langle n_{j\downarrow} \rangle \ . \tag{3.21}$$

Finally, we can obtain in a similar fashion time-dependent correlation functions, by inserting the operators at different points in the product over time slices Eq. (3.8). For example, a time-dependent Green's function is

$$\langle c_i(l_1) c_j^\dagger(l_2) \rangle = \frac{\mathrm{Tr} D_L D_{L-1} \cdots D_{l_1+1} c_i D_{l_1} \cdots D_{l_2+1} c_j^\dagger D_{l_2} \cdots D_1}{\mathrm{Tr} D_L \cdots D_1}$$

$$= \frac{\mathrm{Tr} D_{l_2} \cdots D_1 D_L \cdots D_{l_2+1} [(D_{l_1} D_{l_1-1} \cdots D_{l_2+1})^{-1} c_i D_{l_1} \cdots D_{l_2+1}] c_j^\dagger}{\mathrm{Tr} D_{l_2} \cdots D_1 D_l \cdots D_{l_2+1}} \ . \tag{3.22}$$

By expanding in eigenstates of $D_{l_1} D_{l_1-1} \cdots D_{l_2+1}$, we find

$$(D_{l_1} D_{l_1-1} \cdots D_{l_2+1})^{-1} c_i D_{l_1} D_{l_1-1} \cdots D_{l_2+1} = \sum_k (B_{l_1} B_{l_1-1} \cdots B_{l_2+1})_{ik} c_k \ , \tag{3.23}$$

and replacing in (3.22)

$$\langle c_i(l_1) c_j^\dagger(l_2) \rangle = \sum_k (B_{l_1} B_{l_1-1} \cdots B_{l_2+1})_{ik} \frac{\mathrm{Tr} D_{l_2} \cdots D_1 D_L \cdots D_{l_2+1} c_k c_j^\dagger}{\mathrm{Tr} D_{l_2} \cdots D_1 D_l \cdots D_{l_2+1}} \tag{3.24}$$

and using (3.18), we finally obtain

$$\langle c_i(l_1) c_j^\dagger(l_2) \rangle = \left[B_{l_1} B_{l_1-1} \cdots B_{l_2+1} \frac{1}{1+B_{l_2} \cdots B_1 B_L \cdots B_{l_2+1}} \right] ij \ . \tag{3.25}$$

Similarly,

$$\langle c_i^\dagger(l_1) c_j(l_2) \rangle = \left[\frac{1}{1+B_{l_2} \cdots B_{l_2+1}} B_{l_2} \cdots B_{l_1+1} \right] ij \ , \tag{3.26}$$

and for higher-order correlation functions Wick's theorem applies. From these formulas we can obtain arbitrary correlation functions of interest in the Hubbard model, such as charge and spin correlation functions and susceptibilities.

We have done a variety of checks on our simulation program to make sure it was running properly. For the noninteracting case our results should be exact for a finite lattice, and we have verified this by comparing the results from our simulation program with those obtained from a direct calculation for lattices up to 8×8 in spatial size and various temperatures. For the interacting case, we have earlier reported comparison with exact results for two sites,[14] where we found that the choice $\Delta\tau U = 0.5$ gives reasonable accuracy (within a few percent). In Figs. 4 and 5 we show comparison of our simulation results for the local moment [Eq. (4.1)] and the magnetic susceptibility [Eq. (4.2)] for 6-site rings with the exact results of Shiba.[7] It can be seen that the agreement is excellent. These tests lead us to believe that the results to be presented in the next section for the two-dimensional Hubbard model are reliable.

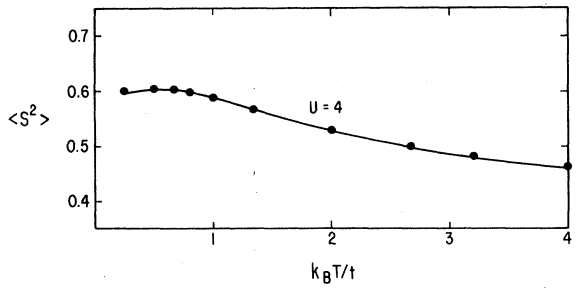

FIG. 4. Local moment versus temperature for a 6-site ring, $U=4$, with $\Delta\tau=0.125$. The solid line is the exact result of Shiba.

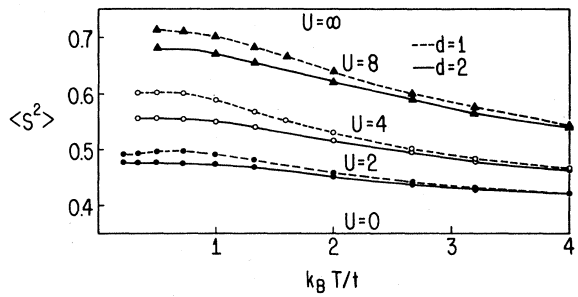

FIG. 6. Local magnetic moment versus temperature on a 6×6 two-dimensional lattice and a 6-site one-dimensional lattice.

IV. RESULTS FOR THE HALF-FILLED-BAND CASE

We have performed simulations in the half-filled-band sector for lattices up to 8×8 in spatial size (with periodic boundary conditions) and interaction strengths $U=2$, 4, and 8. The time slice size was taken to be $\Delta\tau=0.25$, 0.125, and 0.0625 for $U=2$, 4, and 8, respectively. Simulations were performed on a Vax 750 computer and a Cray 1S supercomputer. A sweep through a 6×6 lattice with 32 time slices took 70 sec on the Vax and 0.60 sec on the Cray, plus some fraction of this number depending on the measurements performed. Typically, 200 warm-up and 1000 measurements separated by two sweeps were performed for a given set of parameters. For low temperatures, the algorithm becomes unstable, and the lowest temperature we could study without running into accuracy problems was $\beta=4$ on the Cray (using single precision) and $\beta=4.5$ on the Vax (using double precision). Our program on the Cray with double precision was a factor of 15 to 20 slower so that it was impractical. Because more time slices are needed the larger the interaction and the algorithm becomes unstable more rapidly, we could not reach as low temperatures with $U=8$ as with $U=2$. Also, the statistical error becomes larger the larger the interaction.

Figure 6 shows the local magnetic moment, defined by

$$\langle S^2\rangle=\tfrac{1}{4}\langle\sigma_x^2+\sigma_y^2+\sigma_z^2\rangle=\tfrac{3}{4}\langle\sigma_z^2\rangle\ , \tag{4.1a}$$

$$\sigma_z^1=n_{i\uparrow}-n_{i\downarrow}\ . \tag{4.1b}$$

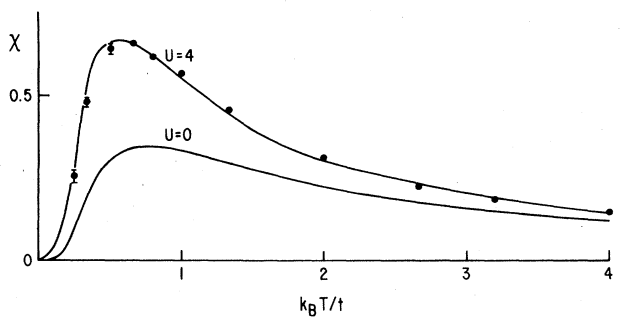

FIG. 5. Magnetic susceptibility versus temperature for a 6-site ring, $U=4$, with $\Delta\tau=0.125$. The solid line is the exact result of Shiba.

The local moment increases gradually as the temperature is lowered, indicating that the electrons are becoming more localized. There is no evidence of any abrupt change as a function of temperature. It also increases gradually as a function of U, and for $U=8$ (equals bandwidth) it is already quite close to the $U=\infty$ value at low temperatures. We also show results for the one-dimensional case for comparison. In units of the bandwidth, the Hubbard interaction is more effective in localizing the electrons as the dimensionality increases.

Figure 7 shows the magnetic susceptibility versus tem-

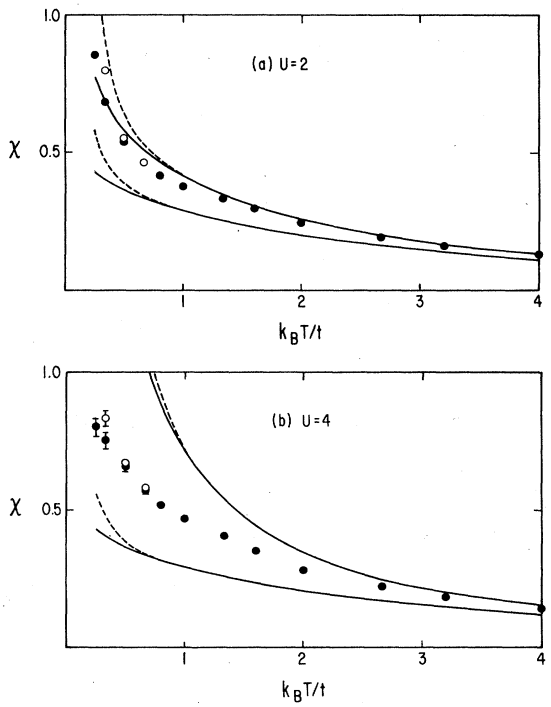

FIG. 7. Magnetic susceptibility versus temperature. The solid circles (open circles) are Monte Carlo results for a 6×6 (4×4) lattice. The lower solid line is the noninteracting result for an infinite lattice, the upper solid line the RPA prediction. The dashed line is the corresponding result for a 6×6 lattice, showing that finite-size effects start to appear around $T\sim0.75$. For the interacting case, finite-size effects appear at a somewhat lower temperature.

perature for $U=2$ and 4. Some results for $U=8$ were given in Ref. 16. The q-dependent (zero-frequency) susceptibility is defined by

$$\chi(q)=\frac{1}{N}\sum_{i,j} e^{iq(R_i-R_j)}\int_0^\beta d\tau\langle[n_{i\uparrow}(\tau)-n_{i\downarrow}(\tau)] \times[n_{j\uparrow}(0)-n_{j\downarrow}(0)]\rangle \quad (4.2)$$

and for $q=0$ it satisfies

$$\chi(q=0)=\beta S(q=0) \quad (4.3)$$

with $S(q)$ the magnetic structure factor,

$$S(q)=\frac{1}{N}\sum_{i,j} e^{iq(R_i-R_j)}\langle(n_{i\uparrow}-n_{i\downarrow})(n_{j\uparrow}-n_{j\downarrow})\rangle\ , \quad (4.4)$$

since the total magnetization commutes with the Hamiltonian. We evaluated the susceptibility using both sides of Eq. (4.3) and found agreement within statistical error. The susceptibility increases smoothly as the temperature is lowered, and there is a slight bulge (particularly for $U=4$) for T between 1 and 2, which is where the local moment is increasing more rapidly. As $T\to 0$, χ diverges logarithmically if $U=0$ [Eq. (2.7)] because of the logarithmic singularity in the density of states, and we expect it to go to zero for large U [Eq. (2.19)]. Although we do not see this behavior up to the lowest temperature studied, χ does increase less rapidly for $U=4$ than for $U=2$ at low temperatures. Except at the lowest temperatures, where the singularity in $\rho(\epsilon)$ plays a role, χ is enhanced more the larger U is, as one would expect. We also show in Fig. 7 the RPA results, Eq. (2.10). From comparison with the Monte Carlo results, we conclude that RPA is fairly accurate for $U=2$, but becomes rapidly inaccurate as U is increased, and it always predicts too large an enhancement of the susceptibility.

Figure 8 shows the staggered magnetic susceptibility versus temperature. Here, for the free case we have the combined effect of the singularity in the density of states and the nested Fermi surface, yielding a low-temperature behavior $\chi_{st}\sim\ln^2(T/t)$. For large U, we expect $\chi_{st}\sim 1/T$ at low temperatures, as discussed in Sec. II. Our results for finite U appear to follow the stronger divergence $\chi_{st}\sim 1/T$. Similarly, as for the susceptibility, RPA overestimates the effect of the interaction, but it is quite accurate for $U=2$ in the temperature range studied. However, RPA predicts a transition to an antiferromagnetic state at $T=0.33$ and 0.75 for $U=2$ and 4, respectively, and we find no evidence for it, as one would expect.

Figure 9 shows the internal energy versus temperature. It is a smoothly varying function of temperature and increases as U is increased. We have extrapolated the ground-state energy assuming a T^2 dependence at low temperature and using our Monte Carlo data for the lowest temperatures. The extrapolated results are $E=-1.17(2)$ for $U=2$, $E=-0.88(3)$ for $U=4$, and $E=-0.48(5)$ for $U=8$. The errors are estimates on the error due to the extrapolation, since the statistical error is very small. The extrapolated data are shown in the inset, where they are compared with results from the Hartree-Fock approximation and an exact lower bound obtained

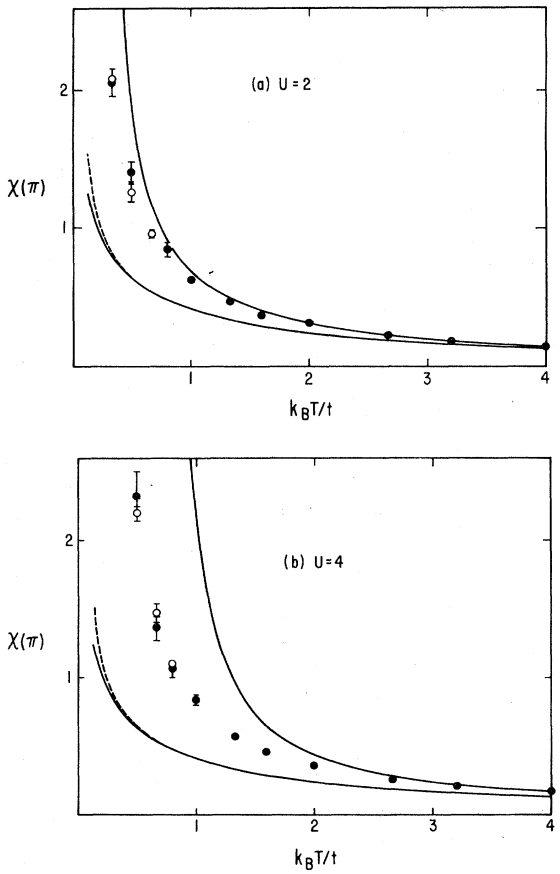

FIG. 8. Same as Fig. 7 for the staggered magnetic susceptibility.

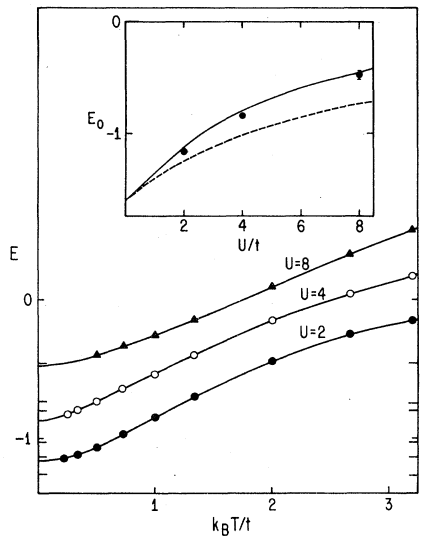

FIG. 9. Energy versus temperature for $U=2$, 4, and 8. The inset shows the extrapolated ground-state energy, compared with Hartree-Fock predictions (solid line) and the Langer-Mattis lower bound (dashed line).

by Langer and Mattis.[22]

At finite temperature, the model considered here cannot undergo a transition to a magnetically ordered state since a continuous symmetry (rotation is spin space) would be broken. At zero temperature, however, the existence of long-range magnetic order is an open question. Although our simulation method cannot deal with $T=0$ directly, we can go to sufficiently low temperatures so that correlations build up over the whole extent of our finite spatial lattice. When the thermal correlation length is larger than the spatial lattice size, the system behaves effectively as if at zero temperature. We can see how the long-range order builds up in the spin-spin correlation function. A picture of the spin-spin correlations $\langle \sigma_z^i \sigma_z^j \rangle$ in real space for an intermediate coupling case ($U=4$) at low temperatures ($\beta=4$) is shown in Fig. 10, on a 8×8 lattice. Note that there are definitely antiferromagnetic correlations extending over the whole lattice. For this low temperature, fluctuations are predominantly quantum rather than thermal (note that the local moment is essentially independent of T for $\beta > 1.5$ in Fig. 5). The reduction in the spin-spin correlation function from the perfect Néel state ($\langle S_z^i S_z^j \rangle = \pm 1$) is due to both charge fluctuations (since $U < \infty$) and spin fluctuations (even for $U \to \infty$, the antiferromagnetic Heisenberg model does not have perfect long-range order). The magnitude of the on-site charge fluctuation can be measured from

$$\langle (n_\uparrow + n_\downarrow)^2 \rangle - \langle n_\uparrow + n_\downarrow \rangle^2 , \tag{4.5}$$

which is zero for $U=\infty$, and 0.5 for $U=0$, and is related to the local moment, Eq. (4.1). For the case shown in Fig. 10, it is 0.26. Another indication that the spins shown in Fig. 10 are not "localized" but "itinerant" is given by the average value of the kinetic energy of the electrons. For the case of Fig. 10, we find

$$\frac{\langle c_{i\sigma}^\dagger c_{j\sigma} \rangle_{U=4}}{\langle c_{i\sigma}^\dagger c_{j\sigma} \rangle_{U=0}} = 0.86 , \tag{4.6}$$

which implies that the electrons are quite delocalized, at least on a short-range basis.

Figure 11 shows the Fourier transform of the spin-spin correlation function

$$S(q) = \frac{1}{N} \sum_{i,j} e^{iq\cdot(\mathbf{R}_i - \mathbf{R}_j)} \langle (n_{i\uparrow} - n_{i\downarrow})(n_{j\uparrow} - n_{j\downarrow}) \rangle \tag{4.7}$$

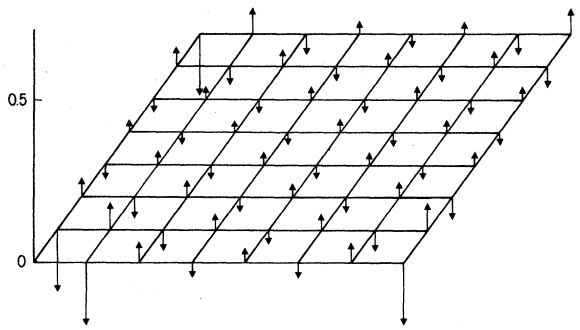

FIG. 10. Spin-spin correlation function for $U=4$ on an 8×8 lattice, $\beta=4$.

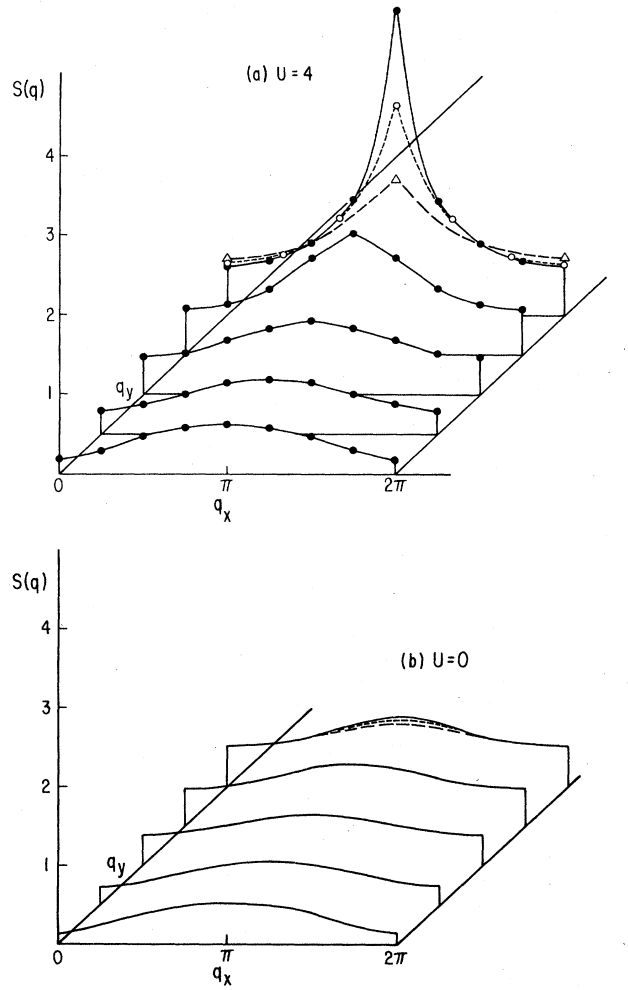

FIG. 11. (a) Magnetic structure factor for $U=4$, on an 8×8 lattice at $\beta=4$ (solid circles), a 6×6 lattice at $\beta=3$ (open circles), and a 4×4 lattice at $\beta=2$ (open triangles). Except where shown, the results for different lattice sizes are identical. (b) Same as (a) for $U=0$, for comparison.

for $U=4$ on an 8×8 lattice with $\beta=4$ (solid line), for a 6×6 lattice, $\beta=3$ (short-dash line), and for a 4×4 lattice, $\beta=2$ (long-dash line). Note how the peak at $\mathbf{q}=(\pi,\pi)$ grows as the lattice size increases and the temperature is lowered. This indicates that the system is developing antiferromagnetic order. The same correlation function for $U=0$ is shown for comparison in Fig. 11(b). For $T=0$, we will have for a sufficiently large lattice

$$S(\pi,\pi) = Nm^2 + S_c(\pi,\pi) , \tag{4.8}$$

with m the staggered magnetization

$$m = \frac{1}{N} \sum_i (-1)^{R_i} \langle n_{i\uparrow} - n_{i\downarrow} \rangle , \tag{4.9}$$

and S_c the connected structure factor. To extrapolate the long-range order, we plot $S(\pi,\pi)/N$ versus $1/N$, following Oitmaa and Betts.[21] According to (4.8), we expect $S(\pi,\pi)/N$ to follow a straight line if plotted versus $1/N$.

From the extrapolated value as $N\to\infty$, we obtain the square of the staggered magnetization. We expect this procedure to work if we are at sufficiently low temperatures such that the thermal coherence length, $v_F\beta$ (v_F denotes Fermi velocity), is much larger than the linear lattice size. We have taken $\beta=0.75\sqrt{N}$, which was close to the lowest temperature we could study without having accuracy problems in the computation of the matrices, and values of $N=8$, 10, 16, 26, and 36. For $N=8$, 10, and 26, we used the "tilted" lattices discussed by Oitmaa and Betts.[21]

Figure 12 shows our results. For $U=0$, the points extrapolate to 0 as they should. For $U=2$ the extrapolation is already clearly finite. The slope of our lines is smaller than the Oitmaa-Betts line, indicating that $S_c(\pi,\pi)$ is smaller. Although our results are certainly a lower bound to the long-range order, there could be some effect of the finite temperature reducing the long-range order, and we believe our results could be underestimating the long-range order by up to 10%. Our results are substantially lower than the Hartree-Fock predictions, due to both charge and spin fluctuations. The fluctuations, however, do not destroy the order as they do in one dimension.

We have attempted to verify the scaling behavior at zero temperature predicted by Hartree-Fock theory for small U, Eq. (2.15), from the numerical simulation. Because the gap is difficult to extract, we focused instead on a spin-spin correlation function at large distances

$$w^2=\langle\sigma_z(0)\sigma_z(N/2)\rangle\ . \tag{4.10}$$

Here, $N/2$ indicates the site that is furthest apart from site 0, and we expect $w\sim m$ for large N. According to HF theory, we would have

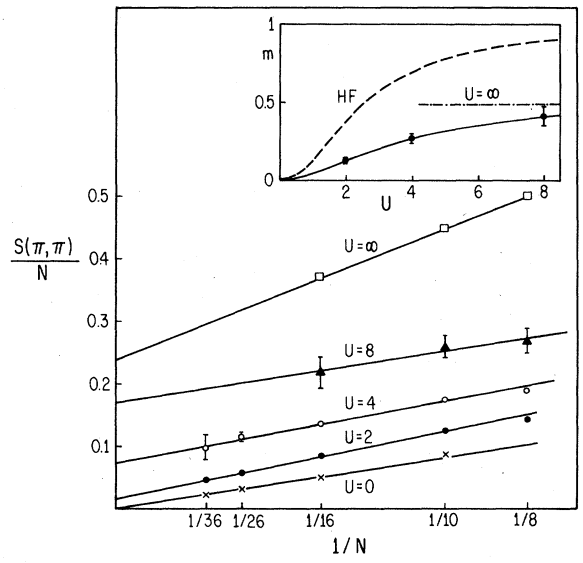

FIG. 12. Extrapolation of long-range antiferromagnetic order. The $U=\infty$ results are taken from Ref. 20. The inset shows the staggered magnetization m versus U, and the Hartree-Fock predictions (dashed line).

$$\Delta^{\rm HF}=Um\sim Uw\sim te^{-2\pi\sqrt{t/U}}\ . \tag{4.11}$$

In one dimension (1D), it is known that the HF gap is

$$\Delta_{\rm 1D}^{\rm HF}\sim te^{-2\pi/U} \tag{4.12}$$

and that fluctuations only modify the prefactor, since the exact gap goes as

$$\Delta_{\rm 1D}\sim\sqrt{Ut}\,e^{-2\pi/U}\ . \tag{4.13}$$

If the same happens in two dimensions (2D), we would have

$$\Delta_{\rm 2D}\sim Uw\sim\sqrt{tU}\,e^{-2\pi\sqrt{t/U}}\ . \tag{4.14}$$

We cannot verify Eqs. (4.11) or (4.14) directly on a small lattice because of finite-size effects. However, we can use a finite-size-scaling analysis. If Eq. (4.11) is valid for an infinite lattice, we expect for a finite lattice of *linear* dimension n:[23]

$$Uw_n=\frac{1}{n}f(ne^{-2\pi\sqrt{t/U}})\ , \tag{4.15}$$

while if (4.14) is valid, we would have

$$\sqrt{U}w_n=\frac{1}{n}f(ne^{-2\pi\sqrt{t/U}})\ . \tag{4.16}$$

To verify (4.16), we plot $\sqrt{U}w_{n_1}$ versus $1/\sqrt{U}$ and $\sqrt{U}w_{n_2}$ versus

$$\frac{1}{\sqrt{U}}-\frac{1}{2\pi}\ln\left[\frac{n_2}{n_1}\right]\ ,$$

for lattices of linear size n_1 and n_2; if (4.16) holds, the results should follow the same curve. If (4.15) holds, this should happen if we plot Uw_n instead.

Figure 13 shows such plots for a 4×4 lattice at $\beta=3$, and a 6×6 lattice at $\beta=4.5$. In Fig. 13(a) we show the results assuming (4.16), while in Fig. 13(c) we check the form (4.15). Our numerical results appear to support the former assumption. In Fig. 13(b) we show scaling for the HF gap on the same finite lattices, as a check on our procedure.

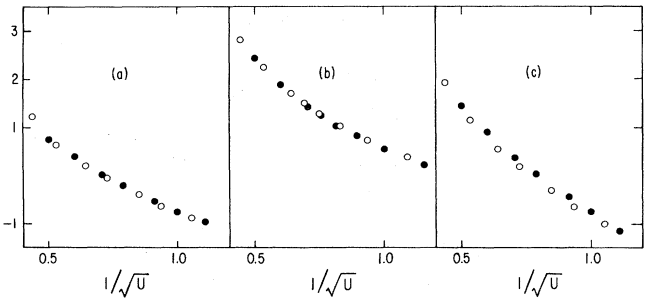

FIG. 13. Finite-size-scaling analysis for small U. (a) $\ln(n\sqrt{U}w_n)$, (b) $\ln(n\Delta_n^{\rm HF})$, and (c) $\ln(nUw_n)$. The solid circles are results for a 4×4 lattice plotted versus $1/\sqrt{U}$, the open circles are results for a 6×6 lattice plotted versus $1/\sqrt{U}-(1/2\pi)\ln\frac{6}{4}$. The points fall on the same curve on (a) but not on (c), indicating that Eq. (4.16) holds.

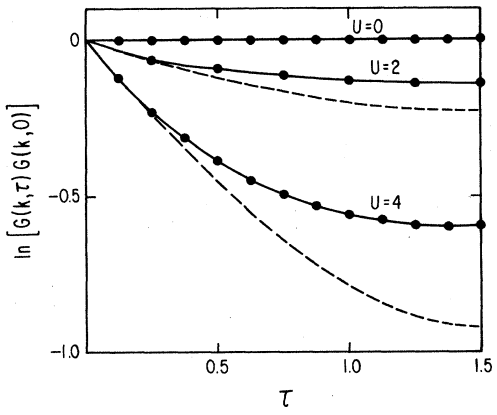

FIG. 14. Imaginary time dependence of Green's function for $k=(\pi/3,2\pi/3)$ 6×6 lattice, $\beta=3$. The dashed lines are the predictions of a rigid two-band picture fitted to the initial time decay.

To summarize, our numerical results suggest that the magnetization for small coupling behaves as

$$m\sim\sqrt{t/U}\,e^{-2\pi\sqrt{t/U}}\ , \tag{4.17a}$$

and assuming the relation $\Delta\propto Um$ between gap and magnetization holds, as in HF theory, we have for the gap in two dimensions,

$$\Delta_{2D}\sim\sqrt{tU}\,e^{-2\pi\sqrt{t/U}}\ , \tag{4.17b}$$

that is, it differs from the HF gap [Eq. (4.11)] by the prefactor only. We cannot completely rule out other possibilities; in particular, our numerical results are not inconsistent with the form $\Delta_{2D}\sim e^{-2\pi t/U}$ (with no U-dependent prefactor). However, we believe that our numerical results together with the HF prediction and the analogy with the one-dimensional case strongly suggest that (4.17) is valid. Further numerical and analytic work should be able to fully resolve this question.

It should be pointed out that the relation (4.17b) follows from (4.17a) only if we make the reasonable assumption that the gap and the magnetization scale in the same way

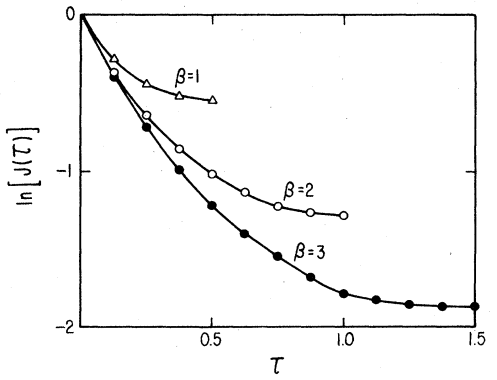

FIG. 15. Imaginary time dependence of current-current correlation function for $U=4$, $\beta=3$, 2, and 1 on a 6×6 lattice.

at zero temperature, but it has not been checked directly. In addition, at finite temperature this relation breaks down, since the magnetization is destroyed by thermal fluctuations while the gap for charge excitations remains. We can see directly that the system develops a gap when U is nonzero by studying the imaginary time decay of various correlation functions. Figure 14 shows the Fourier transform of the time-dependent Green's function

$$G(k,\tau)=\frac{1}{N}\sum e^{ik(R_i-R_j)}\langle c_i(\tau)c_i^\dagger(0)\rangle$$
$$=\langle c_k(\tau)c_k^\dagger(0)\rangle \tag{4.18}$$

at $k=(\pi/3,2\pi/3)$ on a 6×6 lattice. Since this k lies on the Fermi surface for the noninteracting case, the Green's function does not decay for $U=0$. When U is turned on, $G(k,\tau)$ decays, indicating that the system develops a gap for charge excitations. We have attempted to fit the time decay to a simple exponential corrected for finite-temperature effects:

$$G(k,\tau)\propto e^{-\Delta\tau}+e^{-(\beta-\Delta)\tau}\ , \tag{4.19}$$

and to the form predicted by HF theory for $G(k,\tau)$ on a finite lattice at finite temperatures. Both procedures give essentially the same answer and are shown in Fig. 14 as dashed lines, with Δ chosen to fit the initial time decay of $G(k,\tau)$, $\Delta=0.57$ for $U=2$, and $\Delta=1.05$ for $U=4$. The exact results differ markedly from these mean-field results for long times, indicating that a rigid two-band picture is not adequate and that collective charge excitations with a gap smaller than the one predicted by a rigid-band picture exist.

Some mean-field calculations predict that the Hubbard model should undergo a sharp insulator-metal transition as the temperature is increased, leading to a metallic state at high temperatures.[24] We find no evidence for such a transition. Figure 15 shows the imaginary time decay of the current-current correlation function

$$J(\tau)=\langle j_x(\tau)j_x(0)\rangle\ , \tag{4.20a}$$

$$j_x=-i\sum_{i,j,\sigma}(x_i-x_j)c_{i\sigma}^\dagger c_{j\sigma}\ , \tag{4.20b}$$

and x_i the x component of the position vector at site i. The time dependence does not change qualitatively when the temperature is increased, and indicates that there is a finite gap for conductivity at all temperatures. This will give rise to a thermally-activated-type conductivity similar to a semiconductor at all temperatures. Our results support the picture of Bari and Kaplan[25] that the half-filled Hubbard model does not undergo a transition to a metallic state as the temperature is increased.

Finally, it is also interesting to study the occupation number in k space, $\langle c_k^\dagger c_k\rangle=1-G(k)$, at low temperatures. Figure 16 shows results for $\beta=4$ on an 8×8 lattice. The temperature is sufficiently low that the results are very close to the ground-state values. For $U=0$, the occupation number is essentially 1 inside the Fermi surface, 0.5 on the Fermi surface, and 0 outside. Note how the interaction alters this behavior: for $U=4$, the occupation number even at $k=0$ is somewhat smaller than 1.

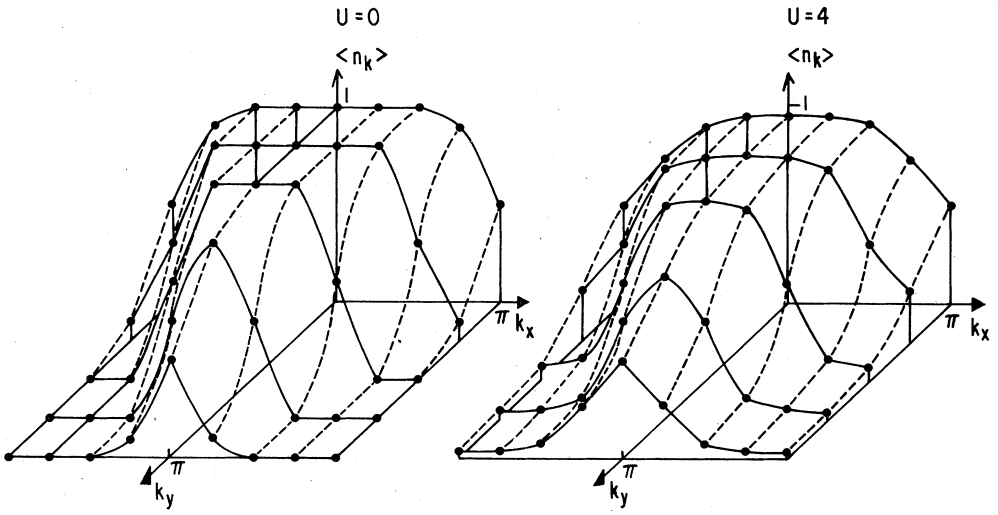

FIG. 16. Occupation number in k space, $n_k=\langle c_k^\dagger c_k\rangle$ on an 8×8 lattice at $\beta=4$. Note how the interaction causes a rounding, and even at $k=0$ the occupation number is less than unity due to the electron-electron interaction.

It is not possible to determine from such a small system whether a well-defined Fermi surface still exists. It is believed, however, from general arguments, that the Fermi surface is destroyed for $U\neq0$, since the system becomes an insulator.

V. NON-HALF-FILLED BAND

We have performed simulations for band fillings other than one-half for $U=4$ and $U=8$. As mentioned in Sec. III, the determinant does become negative for some cases if the band is not half-full, and it becomes necessary to compute the average sign. This happens particularly for large values of the interaction. Table I shows some results for the average sign for various cases. It can be seen that the average sign does become somewhat smaller as the temperature decreases, and does not seem to be very dependent on lattice size. As a function of band filling, it first decreases and then increases again as the band filling is further decreased. For the parameter range studied, the average sign did not become small enough to cause problems in the simulations. It is not clear whether as $\beta\rightarrow\infty$ the average sign vanishes, and if so how. It certainly does not appear to be vanishing exponentially, as in methods where the fermions are not integrated out, but could possibly be vanishing algebraically.

Figure 17 shows the behavior of the spin-spin correlation functions for $U=4$ and several band fillings, for 6×6 lattices at $\beta=4.5$. We also show the results for 4×4, $\beta=3$. Except for the case $\rho=1$, there is essentially no change in the spin-spin correlations in going to larger lattices and decreasing the temperature. This suggests that there is no magnetic order except for $\rho=1$. The peak value shifts from (π,π) as the filling is decreased. The results are very similar to the ones obtained with no correlations except for the $\rho=1$ case.

Figure 18 shows the case $\rho=0.9$ for 4×4 at $\beta=2$; 6×6, $\beta=3$; and 8×8, $\beta=4$. The peak is still at (π,π) here, since we are close to the half-filled band, and there is a small increment in going to larger lattices and increasing β. There is a large difference, however, with the cor-

TABLE I. Average value of the sign of the product of determinants for some cases where the band is non-half-filled. For the half-filled case, the sign is always positive.

U	Band filling	Lattice size	β	⟨Sign⟩
4	0.9	4×4	2	1
			3	0.99
			4	0.94
		8×8	4	0.93
	0.84	4×4	3	0.99
		6×6	4.5	0.77
	0.65	4×4	3	0.99
		6×6	4.5	0.97
	0.48	4×4	3	1
		6×6	4.5	1
8	0.67	4×4	2	0.98
		6×6	3	0.61

TABLE II. On-site and nearest-neighbor spin-spin correlations for $U=8$, $\beta=3$ on a 4×4 lattice for various band fillings. $i+\delta$ denotes a nearest neighbor of site i. The number in parentheses is the statistical error in the last figure.

Band filling	$\langle\sigma_z^2\rangle$	$\langle\sigma_{z,i}\sigma_{z,i+\delta}\rangle$
1	0.899(3)	−0.31(4)
0.91	0.841(4)	−0.21(3)
0.81	0.750(2)	−0.12(4)
0.67	0.636(2)	−0.089(2)
0.60	0.565(2)	−0.079(5)
0.42	0.400(8)	−0.036(7)
0.25	0.247(6)	−0.017(2)

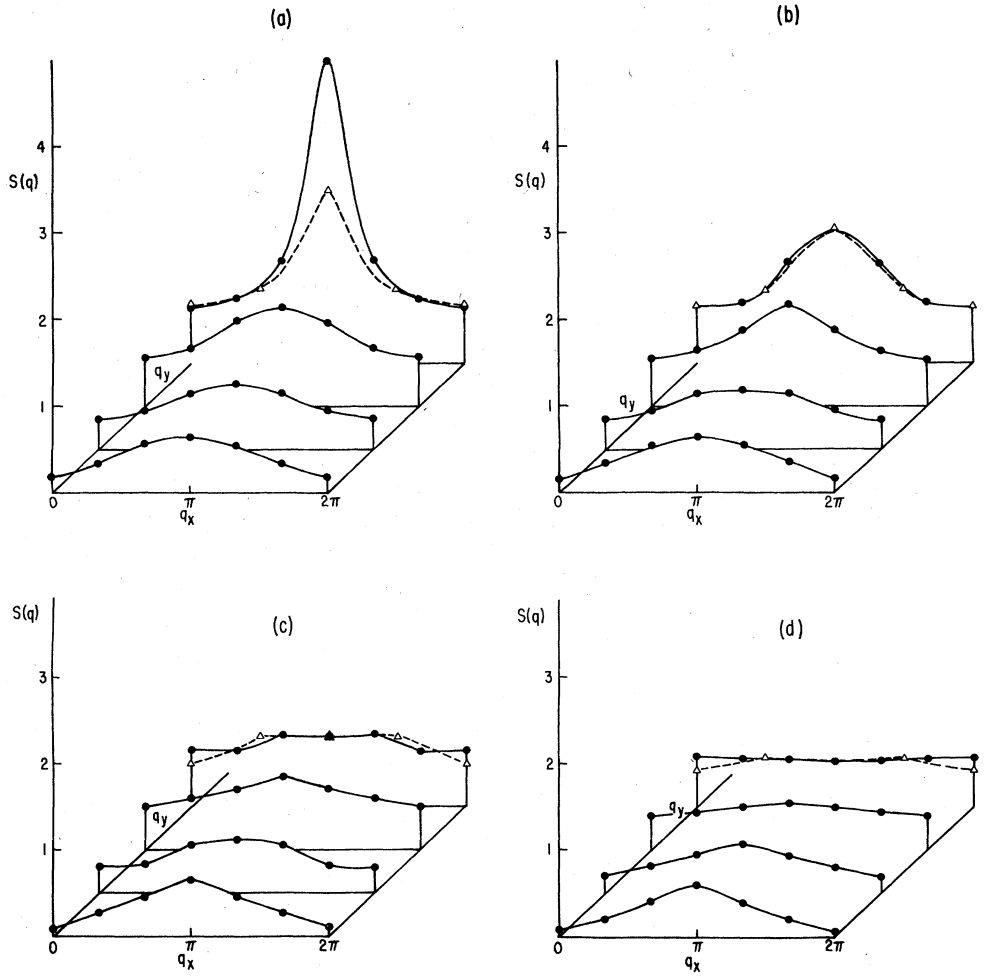

FIG. 17. Magnetic structure factor for $U=4$ on a 6×6 lattice, $\beta=4.5$ (solid lines) and a 4×4 lattice, $\beta=3$ (dashed lines) for several band fillings. (a) $\rho=1$, (b) $\rho=0.84$, (c) $\rho=0.65$, and (d) $\rho=0.48$.

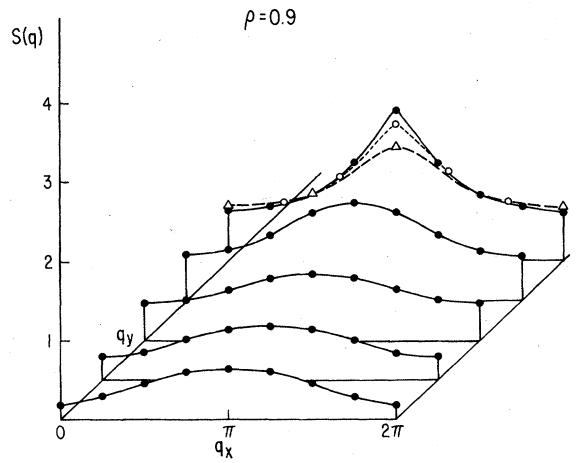

FIG. 18. Magnetic structure factor for $U=4$, $\rho=0.9$ on an 8×8 lattice, $\beta=4$ (solid circles); a 6×6 lattice, $\beta=3$ (open circles); and a 4×4 lattice, $\beta=2$ (open triangles).

responding half-filled case (Fig. 11), while Hartree-Fock theory predicts the antiferromagnetic order for $\rho=0.9$ to be still 75% of the value for $\rho=1$. Also, $S(\pi,\pi)$ appears to be saturating as N and β increase. In Fig. 19 we plot

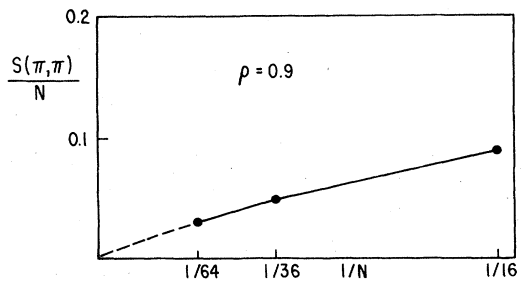

FIG. 19. Extrapolation of long-range antiferromagnetic order for $\rho=0.9$, $U=4$. The results suggest that no long-range order exists.

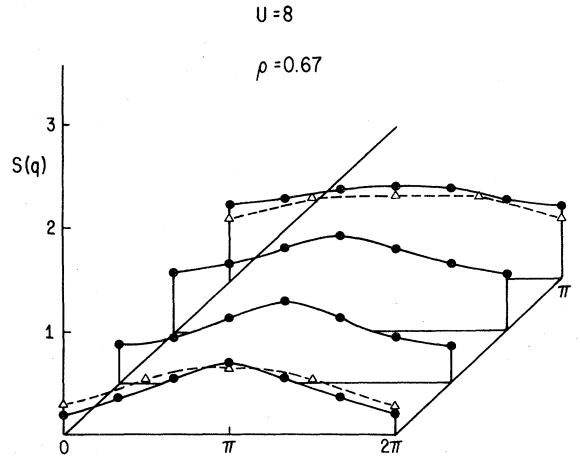

FIG. 20. Magnetic structure factor for $U=8$, $\rho=0.67$ on a 6×6 lattice, $\beta=3$, and a 4×4 lattice, $\beta=2$. Note that there is no indication of ferromagnetism, in contradiction with HF theory.

$S(\pi,\pi)/N$ versus $1/N$ for this case. Although not quite unambiguous, the results suggest that the system does not have antiferromagnetic order in the thermodynamic limit.

We now consider a case which according to mean-field theory should have a ferromagnetic ground state: $U=8$, $\rho=0.65$. The spin-spin correlations in real space show no evidence of even short-ranged ferromagnetic correlations, but rather weak antiferromagnetic correlations. The structure factor is shown in Fig. 20. It has a broad peak at (π,π) but rather weak dependence on lattice size and temperature, suggesting that there is no long-range order here either. In fact, the $q=0$ structure factor *decreases* as the temperature is lowered. We have also explored other band fillings for $U=8$, and found nowhere even short-ranged ferromagnetic correlations. Table II shows the on-site and nearest-neighbor correlations for $U=8$ and several band fillings. It can be seen that the nearest-neighbor correlations are always antiferromagnetic, becoming weaker as the band filling decreases. We conclude that the system shows no tendency for ferromagnetic correlations in the parameter range studied.

Finally, we have also studied pairing correlations in our simulation. We measured the singlet- and triplet-pairing susceptibility, given by

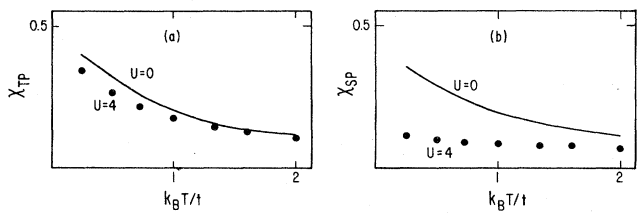

FIG. 21. (a) Triplet- and (b) singlet-pairing susceptibility at $q=0$ versus temperature for $U=0$ and $U=4$, $\rho\sim0.65$.

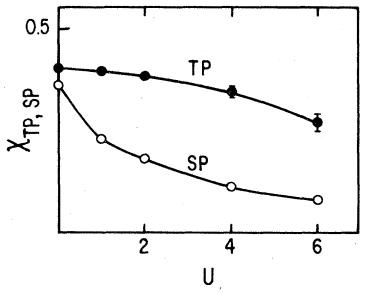

FIG. 22. Triplet- and singlet-pairing susceptibilities at $q=0$ versus U for $\beta=4$, $\rho\sim0.65$.

$$\chi_{SP}(q)=\frac{1}{N}\sum_{i,j}e^{iq(R_i-R_j)}\int_0^\beta d\tau\langle c_{i\uparrow}(\tau)c_{i\downarrow}(\tau)c^\dagger_{j\downarrow}(0)c^\dagger_{j\downarrow}(0)\rangle\ , \tag{5.1}$$

$$\chi_{TP}(q)=\frac{1}{N}\sum_{i,j}e^{iq(R_i-R_j)}\times\int_0^\beta d\tau\langle c_{i\uparrow}(\tau)c_{i+\hat{x},\uparrow}(\tau)c^\dagger_{j+\hat{x},\uparrow}(0)c^\dagger_{j\uparrow}(0)\rangle\ . \tag{5.2}$$

These susceptibilities peak at $q=0$, and diverge if the system undergoes a transition to a singlet or triplet superconducting state. Figure 21 shows the temperature dependence of $\chi_{TP}(q=0)$ and $\chi_{SP}(q=0)$ for $U=0$ and $U=4$, and band filling $\rho\sim0.65$. χ_{SP} is strongly suppressed by U, as one would expect. χ_{TP} for $U=4$ appears to grow in a similar way as for the noninteracting case (χ_{TP} at $U=0$ diverges logarithmically as $T\to0$), but it is smaller at all temperatures. Figure 22 shows the dependence of the triplet- and singlet-pairing susceptibilities on U for $\rho\sim0.65$ at a fixed low temperature; both susceptibilities are suppressed with U, although χ_{SP} much more rapidly. We find also that the suppression is larger for the band closer to half-full. We have also measured the triplet-pairing susceptibility for antiparallel spins, and obtained results very close to χ_{TP}.

Our results for χ_{TP} are surprising, since it has been argued that spin fluctuations should give rise to triplet pairing in a model with strong short-ranged repulsive interactions like the Hubbard model;[26] in particular, it is believed that in ^{3}He the short-ranged repulsion is the dominant mechanism causing superfluidity.[26] Our findings cast doubt on this picture, at least in two dimensions. For the ^{3}He case, we believe that the longer-range attractive tail in the potential is crucial, and simulations on a Hubbard model with nearest-neighbor attractive interactions are in progress.

VI. THE ATTRACTIVE HUBBARD MODEL

We now discuss briefly the properties of the attractive Hubbard model in the half-filled-band case. We can do this without extra work, since as is well known, a

particle-hole transformation can map $U>0$ into $U<0$. The transformation is[27]

$$d_{i\uparrow}=c_{i\uparrow}\ ,$$
$$d_{i\downarrow}=c_{i\downarrow}^{\dagger}(-1)^{i}\ , \tag{6.1}$$

which takes $U\rightarrow -U$ and leaves the kinetic energy invariant. Under this transformation, S_z-S_z correlations are mapped onto charge-density correlations:

$$n_{i\uparrow}-n_{i\downarrow}\rightarrow n_{i\uparrow}+n_{i\downarrow}\ , \tag{6.2}$$

so that long-range antiferromagnetic order corresponds to a charge-density-wave (CDW) state. We have also, however, long-range antiferromagnetic order in the other directions of spin space; the spin operator in the x direction, for example, is

$$S_x^i=c_{i\uparrow}^{\dagger}c_{i\downarrow}+c_{i\downarrow}^{\dagger}c_{i\uparrow}\rightarrow d_{i\uparrow}^{\dagger}d_{i\downarrow}^{\dagger}+d_{i\downarrow}d_{i\uparrow}\ , \tag{6.3}$$

and long-range order in the x component of the spin corresponds to long-range singlet superconducting order in the attractive case. We conclude then that the ground state of the two-dimensional attractive Hubbard model (half-filled) is very peculiar in that it exhibits simultaneously CDW and superconducting long-range order. In the presence of any small perturbation, for example, a longer-range electron-electron interaction, one of the types of order will probably be destroyed and the other further stabilized. This is an interesting question to explore further.

VII. CONCLUSIONS

We have studied properties of the two-dimensional Hubbard model on a square lattice using Monte Carlo simulations. As mentioned in Sec. II, we expect some of the features found here to be very specific to the model studied and others to be more general. The purpose of this study was to provide answers to the following questions. (a) What are the properties of the simplest lattice model of interacting electrons in two dimensions? (b) How useful is the Hubbard model to describe electron correlations and its consequences for narrow-band systems? And, (c) how well does mean-field theory describe the model? We believe we have provided at least partial answers to these questions. Finally, another purpose of our work was to demonstrate that numerical simulations can be a useful tool to study interacting electron systems in more than one dimension.[28]

Our conclusions can be summarized by the phase diagram in Fig. 23. We have shown that for the half-filled band case the system exhibits antiferromagnetic long-range order for all values of the interactions. This conclusion is by no means obvious: In the $U=\infty$ limit, spin fluctuations reduce the long-range order to 50% of its classical value, as shown by Betts and Oitmaa; one might have expected that for any $U<\infty$, charge fluctuations destroy the order altogether, or that a critical value U_c exists below which no long-range order exists. Even though the susceptibility diverges for $U=0$, this does not prove that long-range order exists for any $U>0$; recall the case of one-dimensional spinless fermions with a nearest-neighbor repulsion V, where, even though the $V=0$ susceptibility is divergent, long-range order starts building up only for $V\geq 2t$. Our numerical results indicate that long-range order exists for any value of $U>0$, although substantially reduced from the mean-field-theory predictions. We have also studied the character of the transition at zero coupling using finite-size scaling, and concluded that the mean-field-theory predictions are essentially correct except for a prefactor, as occurs in one dimension.

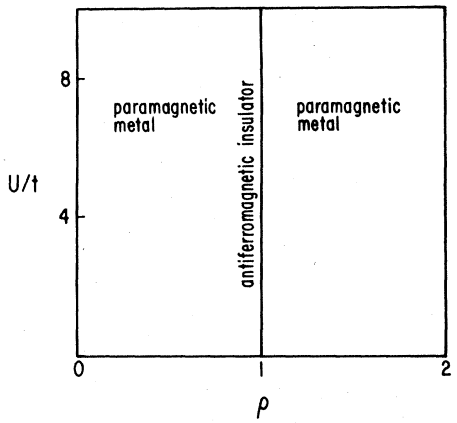

FIG. 23. Conjectured ground-state phase diagram for the two-dimensional Hubbard model.

For the non-half-filled band, although we have only explored a few points on the phase diagram, we believe our results strongly suggest that no long-range magnetic order exists. We have also found no indication of even short-ranged ferromagnetic correlations. Concerning this last point, our findings are in agreement with those of other authors,[10] who suggested that bipartite lattices are particularly unfavorable for ferromagnetic correlations.

Unfortunately, our phase diagram, Fig. 23, is much less interesting than the Hartree-Fock phase diagram, Fig. 3. It appears that an approximate (and qualitatively wrong) solution to a simple model does much better in describing features of real materials than the exact solution of the model. In fact, our model does not really describe itinerant magnetism: only for the insulating case do we find magnetic long-range order. Although this could be due to dimensionality (work on the three-dimensional Hubbard model is in progress), it is possible that a model to describe itinerant magnetism will have to necessarily include band degeneracy.

We have also explored pairing correlations and, in particular, triplet pairing. Recently, it has been suggested that triplet superconductivity could occur in strongly interacting fermion systems, driven by an electronic interaction mechanism.[29] Our results suggest that this is unlikely in a single-band model; it could, however, conceivably occur in models with more than one band.

Several questions about the two-dimensional Hubbard model remain open. The consequences of the singularity in the density of states coinciding with the nesting of the Fermi surface should be investigated theoretically beyond the RPA: a renormalization-group treatment appears possible. For strong coupling, the formulation we have

used breaks down because of the finite time step $\Delta\tau$. In that regime, it should be more useful to construct first an effective Hamiltonian, valid to some order in t/U, to be studied directly by numerical simulations. Questions such as the range of validity of Nagaoka's theorem could then be addressed. Finally, changing the band structure by introducing, for example, a next-nearest-neighbor hopping term should lead to new and interesting physics. In particular, it will produce the singularity in the density of states to occur at an energy where nesting does not occur. This could possibly lead to ferromagnetism if the Fermi energy coincides with the singularity in the density of states. It could also lead to superconductivity if an effective attractive interaction between the electrons exists caused by coupling to boson degrees of freedom. In addition, since nesting will not occur in the half-filled case, it could lead to a Mott metal-insulator transition for a finite value of the interaction.

ACKNOWLEDGMENTS

I am grateful to the Condensed Matter Sciences Division at Los Alamos National Laboratory for providing funds for use of the Cray, to the Center of Nonlinear Studies at Los Alamos for its hospitality, and in particular to D. Campbell and J. Gubernatis for their assistance. I am also grateful to D. J. Scalapino for stimulating discussion. This work was supported by the National Science Foundation under Grant No. DMR-82-17881.

APPENDIX

We discuss here an elementary derivation of Eq. (3.9). It follows from the identity:

$$\mathrm{Tr} e^{-c_i^\dagger A_{ij} c_j} e^{-c_i^\dagger B_{ij} c_j} = \det(1+e^{-A}e^{-B}) , \tag{A1}$$

where A and B are arbitrary matrices, and the summation over indices is understood. To prove (A1), we first prove the identity:

$$e^{-c_i^\dagger A_{ij} c_j} e^{-c_i^\dagger B_{ij} c_j} = e^{-\sum_\nu c_\nu^\dagger l_\nu c_\nu} , \tag{A2}$$

where $\lambda_\nu = e^{-l_\nu}$ are the eigenvalues of the matrix $e^{-A}e^{-B}$. From (A2), Eq. (A1) follows immediately, since

$$\begin{aligned} \mathrm{Tr} e^{-\sum_\nu c_\nu^\dagger l_\nu c_\nu} &= \mathrm{Tr} \prod_\nu e^{-c_\nu^\dagger l_\nu c_\nu} \\ &= \prod_\nu (1+e^{-l_\nu}) \\ &= \det(1+e^{-A}e^{-B}) . \end{aligned} \tag{A3}$$

To prove (A2), we show that an arbitrary many-particle state propagates in the same way using the expression on either side. Consider first a single-particle state

$$|\phi\rangle = \sum_j a_j c_j^\dagger |0\rangle \tag{A4}$$

with a_j arbitrary numbers, and $|0\rangle$ the vacuum state. Let $|\mu\rangle$ be the basis where the matrix B is diagonal, i.e.,

$$B = \sum_\mu |\mu\rangle b_\mu \langle\mu| , \tag{A5}$$

and define new fermion coordinates

$$\begin{aligned} c_\mu &= \sum_j \langle\mu|j\rangle c_j , \\ c_\mu^\dagger &\sum_j \langle j|\mu\rangle c_j^\dagger , \end{aligned} \tag{A6a}$$

with inverse

$$\begin{aligned} c_j &= \sum_\mu \langle j|\mu\rangle c_\mu , \\ c_j^\dagger &= \sum_\mu \langle\mu|j\rangle c_\mu^\dagger . \end{aligned} \tag{A6b}$$

We can write the exponential of B, using the properties of fermion operators, as

$$e^{-c_i^\dagger B_{ij} c_j} = e^{-c_\mu^\dagger b_\mu c_\mu} = \prod_\mu [1+(e^{-b_\mu}-1)c_\mu^\dagger c_\mu] . \tag{A7}$$

On applying this to the state (A4), expanding $c_j^\dagger$ in terms of $c_\mu^\dagger$, and using fermion anticommutation relations, we find

$$\begin{aligned} e^{-c_i^\dagger B_{ij} c_j}|\phi\rangle &= \sum_j a_j' c_j^\dagger |0\rangle , \\ a_i' &= \sum_j (e^{-B})_{ij} a_j . \end{aligned} \tag{A8}$$

Similarly, in operating with both factors on the left-hand side of Eq. (A2), one finds after some algebra

$$\begin{aligned} e^{-c_i^\dagger A_{ij} c_j} e^{-c_i^\dagger B_{ij} c_j}|\phi\rangle &= \sum_j a_j'' c_j^\dagger |0\rangle , \\ a_i'' &= \sum_j (e^{-A}e^{-B})_{ij} a_j , \end{aligned} \tag{A9}$$

i.e., the amplitude of the propagated state is obtained by multiplying the original amplitude by the *product* of the matrices. Equation (A9) is valid in any basis, in particular in the one where $e^{-A}e^{-B}$ is diagonal. If we start then with a state that is an eigenstate of $e^{-A}e^{-B}$:

$$|\phi\rangle = c_\nu^\dagger |0\rangle ,$$

then

$$e^{-c_i^\dagger A_{ij} c_j} e^{-c_i^\dagger B_{ij} c_j} = (e^{-A}e^{-B})_{\nu\nu} c_\nu^\dagger |0\rangle = e^{-l_\nu} c_\nu^\dagger |0\rangle ,$$

which is the same of course as we obtain from the right-hand side of Eq. (A2), using the relation (3.16). Thus, we have proved Eq. (A2) when applied to single-particle states, and it only remains to be shown that if we have more than one particle they propagate independently. Consider first the propagation by one factor. If we take a two-particle state

$$|\phi\rangle = c_{\mu_1}^\dagger c_{\mu_2}^\dagger |0\rangle \tag{A10}$$

and propagate it with B, we have

$$e^{-c_i^\dagger B_{ij} c_j}|\phi\rangle = \prod_\mu [1+(e^{-B_\mu}-1)c_\mu^\dagger c_\mu] c_{\mu_1}^\dagger c_{\mu_2}^\dagger |0\rangle$$
$$= e^{-B_{\mu_1}} e^{-B_{\mu_2}} c_{\mu_1}^\dagger c_{\mu_2}^\dagger |0\rangle \ . \quad \text{(A11)}$$

Equation (A11) clearly holds if $\mu_1 \neq \mu_2$, since we pair μ_1 and μ_2 with its corresponding factor, and also if $\mu_1 = \mu_2$, since then both sides are zero due to the Pauli principle. Clearly then, the propagation of an arbitrary two-particle state is a superposition of the propagation of each particle independently, and similarly for many-particle states. By using the argument repeatedly, it follows also for propagation through more than one factor, which completes the proof of Eq. (A1). Of course, this is then trivially extended to more than two factors.

[1]J. Hubbard, Proc. R. Soc. London, Ser. A **276**, 283 (1963); **281**, 401 (1964).

[2]See, for example, *Electron Correlation and Magnetism in Narrow-Band Systems,* edited by T. Moriya (Springer, New York, 1981), and references therein.

[3]E. Lieb and F. Wu, Phys. Rev. Lett. **20**, 1445 (1968).

[4]D. Penn, Phys. Rev. **142**, 350 (1966).

[5]M. Cyrot, J. Phys. (Paris) **33**, 125 (1972).

[6]M. C. Gutzwiller, Phys. Rev. **137**, A1726 (1965).

[7]H. Shiba and P. Pincus, Phys. Rev. B **5**, 1966 (1972); H. Shiba, Prog. Theor. Phys. **48**, 2171 (1972).

[8]Z. G. Soos and S. Ramasesha, Phys. Rev. B **29**, 5410 (1984).

[9]A. Kawabata, in Ref. 2, p. 172.

[10]M. Takahashi, J. Phys. Soc. Jpn. **51**, 3475 (1982).

[11]J. E. Hirsch, D. J. Scalapino, R. L. Sugar, and R. Blankenbecler, Phys. Rev. B **26**, 5033 (1982).

[12]J. E. Hirsch and D. J. Scalapino, Phys. Rev. B **27**, 7169 (1983); **29**, 5554 (1984).

[13]J. E. Hirsch, Phys. Rev. Lett. **53**, 2327 (1984), and unpublished.

[14]J. E. Hirsch, Phys. Rev. B **28**, 4059 (1983).

[15]R. Blankenbecler, D. J. Scalapino, and R. L. Sugar, Phys. Rev. D **24**, 2278 (1981); D. J. Scalapino and R. L. Sugar, Phys. Rev. B **24**, 4295 (1981).

[16]J. E. Hirsch, Phys. Rev. Lett. **51**, 1900 (1983).

[17]See, for example, P. M. Chaikin, P. Pincus, and G. Beni, J. Phys. C **8**, L65 (1975); P. Richmond, Solid State Commun. **7**, 997 (1969); D. Mattis and W. Langer, Phys. Rev. Lett. **25**, 376 (1970).

[18]S. Doniach and E. Sondheimer, *Green's Functions for Solid State Physicists* (Benjamin, Reading, Mass., 1982), p. 162.

[19]This feature was also found recently by J. Gubernatis, D. Scalapino, R. Sugar, and D. Toussaint (private communication) in a two-dimensional spin-polarized fermion model, where it causes an enhanced tendency to charge-density-wave formation.

[20]Y. Nagaoka, Phys. Rev. **147**, 392 (1966).

[21]J. Oitmaa and D. Betts, Can. J. Phys. **56**, 897 (1978).

[22]W. D. Langer and D. C. Mattis, Phys. Lett. **36A**, 139 (1971).

[23]H. H. Roomany and H. W. Wyld, Phys. Rev. D **21**, 3341 (1980).

[24]S. Doniach, Adv. Phys. **18**, 819 (1969), and references therein.

[25]R. Bari and T. Kaplan, Phys. Rev. B **6**, 4623 (1972).

[26]K. Levin and O. T. Valls, Phys. Rep. **98**, 1 (1983), and references therein.

[27]V. J. Emery, Phys. Rev. B **14**, 2989 (1976).

[28]Results of simulations of a two-dimensional spin-polarized fermion model have been recently reported by D. Scalapino, R. Sugar, and W. Toussaint, Phys. Rev. B **29**, 5253 (1984).

[29]P. W. Anderson, Phys. Rev. B **30**, 1549 (1984).